

# The effect of the relative orientation between the coronal field and new emerging flux: I Global Properties

K. Galsgaard<sup>1</sup>, V. Archontis<sup>4</sup>, F. Moreno-Insertis<sup>2,3</sup> and A. W. Hood<sup>4</sup>

## ABSTRACT

The emergence of magnetic flux from the convection zone into the corona is an important process for the dynamical evolution of the coronal magnetic field. In this paper we extend our previous numerical investigations, by looking at the process of flux interaction as an initially twisted flux tube emerges into a plane parallel, coronal magnetic field. Significant differences are found in the dynamical appearance and evolution of the emergence process depending on the relative orientation between the rising flux system and any preexisting coronal field. When the flux systems are nearly anti-parallel, the experiments show substantial reconnection and demonstrate clear signatures of a high temperature plasma located in the high velocity outflow regions extending from the reconnection region. However, the cases that have a more parallel orientation of the flux systems show very limited reconnection and none of the associated features. Despite the very different amount of reconnection between the two flux systems, it is found that the emerging flux that is still connected to the original tube, reaches the same height as a function of time. As a compensation for the loss of tube flux, a clear difference is found in the extent of the emerging loop in the direction perpendicular to the main axis of the initial flux tube. Increasing amounts of magnetic reconnection decrease the volume, which confines the remaining tube flux.

*Subject headings:* Sun: magnetic fields – Numerical experiments – Sun: active regions – Sun: corona

## 1. Introduction

Flux emergence is one of the manifestations of the continuously changing solar magnetic field. In this process magnetic flux is transported up through the convection zone presumably by a combination of buoyancy and convection towards the photosphere. At the photosphere the physical structure of the sun changes, from a convectively unstable to a convectively stable atmosphere, making the continued rise of magnetic flux, due to buoyancy, more difficult. Despite this, numerous observations in all wavelength ranges show that the emergence process is a frequently occur-

ring event in the solar atmosphere.

There are numerous observations of the photosphere and lower transition region (Lites et al. 1995, 1998; Strouse & Zwaan 1999; Kubo et al. 2003; Pariat et al. 2004; Lites 2005). These show a picture whereby emerging magnetic fields change the convective flows, allowing for initially horizontal magnetic fields to penetrate the photosphere. As the magnetic field expands into the transition region and lower corona, relatively cold plasma is lifted by the magnetic field and eventually starts draining back towards the photosphere, along the magnetic field lines. In isolated emergence events two strong opposite polarities arise forming two magnetically connected sunspots. In the region between the two flux concentrations new flux continues to emerge, with new positive - negative pairs arising at different positions. Lites et al. (1995) used observations covering temperatures from photosphere to corona plasma to argue that a full coherent flux tube rises from the convection

<sup>1</sup>Niels Bohr Institute, Julie Maries vej 30, 2100 Copenhagen Ø, Denmark

<sup>2</sup>Instituto de Astrofísica de Canarias (IAC), Via Lactea s/n, 38200 La Laguna (Tenerife), Spain

<sup>3</sup>Department of Astrophysics, Faculty of Physics, Universidad de La Laguna, 38200 La Laguna (Tenerife), Spain

<sup>4</sup>School of Mathematics and Statistics, University of St Andrews, North Haugh, St Andrews, Fife KY16 9SS, UK

zone. Stroupe & Zwaan (1999) suggested that the flux emerges in "parallel" sheets between the two major flux concentrations, and that the random appearance of new small flux concentrations between the two sunspots favor a picture whereby undulating field lines emerge at different locations along the full length of the field line connecting the two sunspots. Pariat et al. (2004) uses field extrapolation of the photospheric field to establish a field line structure of the magnetic field and find that undulating field lines exist in this model. Furthermore, the dips are associated with Ellerman bombs (Georgoulis et al. 2002), and they interpret these as being responsible for leaving dense material in the part of the loop that dips below the photosphere, making the emergence for the remaining upper part of the loop much easier.

The manifestation of flux emergence in the solar corona often results in a strong interaction between the two initially disconnected flux systems. This interaction results in local brightenings observed in all wavelengths from white light through EUV and into X-ray. Often these events are associated with high-speed flows of the hot plasma emerging from the (reconnection) region where the two flux systems interact. Longcope et al. (2005) investigated one such event. Using simple flux estimates for the flaring structures, they showed how the new flux regions changed its connectivity with time and became connected to the existing coronal magnetic field. This happened in such a way that no dynamic activity took place for a initial period of time, followed by a rapid change of connectivity, and finally a more quiet phase.

How does this interaction depend on the structure of the two initially separate flux systems? No clear analysis has been made on existing observational data, and one can ask if this is actually possible, with the present inability of directly tracking magnetic field lines and their photospheric connections. Further to this, each observed event is different from previous ones in a number of ways, so how can one quantify the most important reasons for these differences in evolution?

Such effects are much easier to investigate by undertaking a series of numerical experiments where one can control, in detail, the environment into which the flux emergence occurs. In previous experiments (Fan 2001; Magara & Longcope 2003; Archontis et al. 2004, 2005; Manchester et al.

2004; Magara 2006), the rise of a twisted loop is initiated inside the convection zone and followed in a self-consistent manner. In these investigations, the structure of the emerging flux resembles a situation where the outer layers of the flux tube expand into the corona. In a manner, this resembles the process of peeling off the outer layers of an onion and expanding these parts into the corona. Specifically Magara (2006), compared the development of the photospheric flux concentrations with observations, finding the same characteristic evolution of the flux concentrations and their associated inversion polarity line as seen in observations. Galsgaard et al. (2005); Archontis et al. (2005) and Isobe et al. (2005) presented the first 3D MHD experiments in which a twisted flux tube emerges from the convection zone and interacts with a pre-existing coronal magnetic field.

Archontis et al. (2005) analyzed in detail the interaction between an emerging magnetic flux system and a uniform horizontal coronal magnetic field, using for the rising tube the same initial conditions as in previous experiments (e.g. Fan (2001); Archontis et al. (2004)). Archontis et al. (2005) show how the sub-photospheric flux tube emerges into the corona and pushes the magnetic field upward and outward. Given the initial almost antiparallel, mutual orientation of the system at the time of first contact, a strong current sheet is formed at the interface. The interaction of the two flux systems then follows a complicated pattern that slowly changes in time. This interaction depends also on the relative orientation between the two systems, as has been pointed out by Galsgaard et al. (2005).

In a different approach, Fan & Gibson (2004) used a 2D magnetic arcade field embedded in a constant temperature coronal region, into which they force a pre-defined curved loop structure using an imposed boundary electric field. This showed, for the setup with minimal reconnection between the two flux systems, that the twisted emerging loop entered into the "corona", eventually experienced a kink instability and strong currents were generated where reconnection takes place due to non-ideal effects. The emergence of a twisted loop into the corona is supported by Lites et al. (1995). Therefore it is interesting to compare the structure of current concentrations between Fan & Gibson (2004) and exper-

iments which included the full emergence process, knowing that differences in the coronal structure and the emergence process may provide very different dynamical evolutions.

In this paper, we follow up on the work presented in Galsgaard et al. (2005) and Archontis et al. (2005) and investigate, in more detail, the significant deviations in the emergence process as the orientation between the two interacting magnetic flux systems is changed. In Section 2 we briefly describe the numerical model. Sections 3-6 contain the various results of the experiments and Section 7 is a discussion of the implications of these results. Finally, highlights of the results are summarized in Section 8.

## 2. Model setup and numerical approach

The parameters of the magnetic flux tube, the background stratification and the initial conditions follow the work presented in Galsgaard et al. (2005) and Archontis et al. (2005). As a reference for the following discussion we start by summarizing the initial state of the experiments and the numerical approach.

Our model consists of a highly stratified environment and a horizontally twisted magnetic tube. The background medium consists of an adiabatically stratified convection zone, an isothermal layer representing the photosphere, a region where the temperature steeply increases with height and represents the transition region and finally an isothermal layer with coronal temperatures. The tube center is located almost 2 Mm below the base of the photosphere. The longitudinal component of the magnetic tube has a Gaussian profile with a central field strength of 3.8 kG, while the twist is uniform around the axis of the tube. This particular flux tube is stable towards the kink instability. This gives a plasma  $\beta = 12.8$  at the axis of the tube. The rise of the tube is triggered by implementing a density deficit distribution that has a maximum at the middle of the axis of the tube and with a Gaussian distribution along the tube. Initially, a horizontal magnetic field is included in the atmosphere above the lower transition region. The orientation of the ambient field relative to the main axis of the tube is an important parameter in the experiments.

Figure 1 shows the gas pressure, temperature

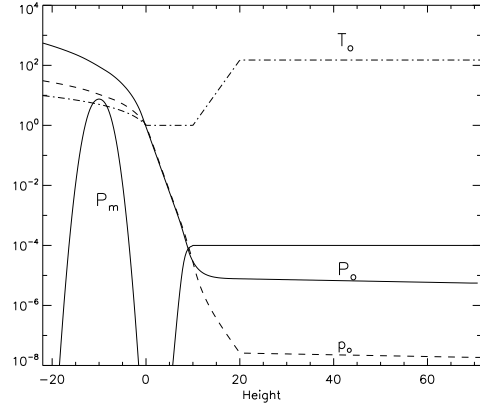


Fig. 1.— Distribution of gas pressure (thick solid), density (dashed), temperature (dash-dotted) and magnetic pressure (thin solid) along the central, vertical ( $y = 0, x = 0$ ) line.

and density of the stratified environment as a function of height. All the profiles are normalized according to the photospheric values:  $p_{ph} = 1.4 \cdot 10^5$  erg cm $^{-3}$ ;  $\rho_{ph} = 3 \cdot 10^{-7}$  g cm $^{-3}$ ;  $T_{ph} = 5.6 \cdot 10^3$  K and  $H_{ph} = 170$  km. Other units used in the simulations are: time,  $t_{ph} = 25$  sec; velocity,  $V \equiv (p_{ph}/\rho_{ph})^{1/2} = 6.8$  km sec $^{-1}$  and magnetic field,  $B_{ph} = 1.3 \cdot 10^3$  Gauss.

The distribution of the magnetic pressure in Fig. 1 shows the magnetic flux tube and the ambient field. The ambient field is given by

$$\mathbf{B}_{cor} = B_c(z) [\cos(\phi), \sin(\phi), 0], \quad (1)$$

where  $B_c(z)$  is described by an hyperbolic tangent profile. The intensity of the coronal field is chosen such that the local plasma  $\beta$  is close to 0.06.

The direction of the initial ambient field is given by the polar angle  $\phi$ , which is measured in a horizontal  $xy$ -plane from the positive  $x$ -axis. At the same time the magnetic fieldlines at the top of the rising flux system are oriented in an approximately antiparallel direction to the ambient fieldlines when  $\phi = 0$  and they are almost parallel when  $\phi = 180$  (see Fig. 2). Thus, the relative horizontal angle between the two flux systems upon contact is  $\phi_0 = 180 - \phi$  deg. The polar angle,  $\phi$ , of the coronal magnetic field is different in the five experiments we have performed; it changes from  $\phi = 0$  to  $\phi = 180$  (see Table (1)).

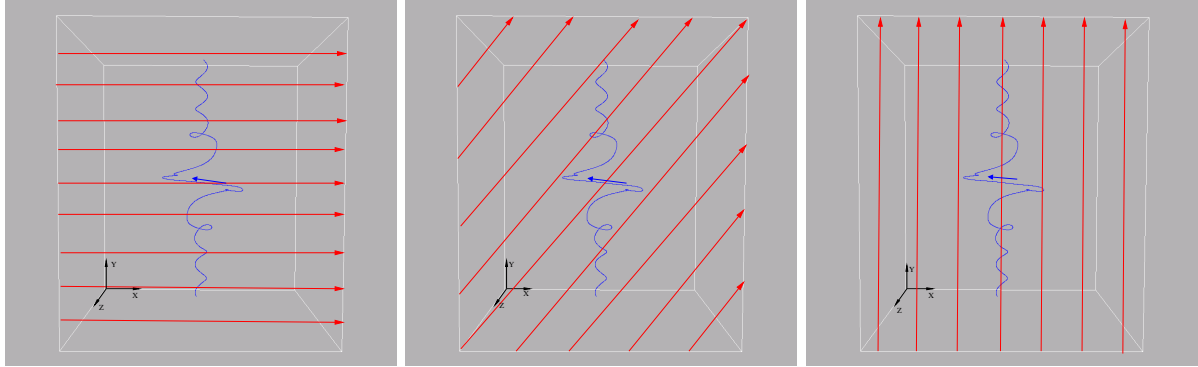


Fig. 2.— Top view of an emerging twisted fieldline and the ambient coronal field (long horizontal arrows). The short arrow at the center of the box shows the direction of the emerging fieldline. The three panels represent different relative orientations of the two flux systems: experiment A:  $\phi = 0$ , experiment B:  $\phi = 45$  and experiment C:  $\phi = 90$ .

Experiment	$\phi_0$	Line style	Orientation
A	180.	Triple Dotted dashed	Antiparallel
B	135.	Dot-Dashed	Slanted
C	90.	Full	Perpendicular
D	45.	Long-Dashed	Slanted
E	0.	Dotted	Parallel

Table 1: List of the numerical experiments performed in the simulations. The first column shows the reference names of the experiments. The second column shows the relative horizontal angle of the two magnetic systems. The third column indicates the linestyle used in the different plots in this paper and the fourth column the orientation of the coronal field relative to the upcoming field.

The evolution of the system is governed by the three-dimensional, time-dependent and resistive MHD equations. These are solved using a numerical approach based on high order finite differencing on staggered grids. By using 6 neighboring data points, a 6th order accurate spatial derivatives and corresponding 5th order accurate interpolations routines are used. The solution is advanced in time using a 3rd order predictor-corrector algorithm. Due to the high spatial order, special treatment of viscosity and resistivity are required to prevent numerical ringing in the vicinity of steep gradients in the physical quantities. This is handled by a combined approach, that is designed to remove numerical problems that can occur in specific problems. These approaches are localized in space, implying that dissipation only take place over length scales of a few gridpoints. Using such an approach, makes it impossible to

assign a single characteristic Reynolds number for the experiment (Nordlund & Galsgaard 1997).

The numerical resolution of the experiments is (148, 160, 218) in the  $(x, y, z)$  directions, with  $z$  being the height. The size of the numerical domain is  $(-60, 60)$ ,  $(-70, 70)$  and  $(-22, 70)$ , which is equivalent to a box of sides 20.4 Mm x 23.8 Mm x 15.6 Mm. The resolution in the  $x$  and  $y$  directions is 137.8 km/cell and 148.8 km/cell correspondingly. The grid in the vertical direction is stretched in a way that the highest resolution covers the region from the top of convection zone to the bottom of the corona. Here the grid resolution is 47.7 km/cell. The resolution has lower values close to the top and bottom boundary of the numerical domain.

### 3. Current sheet orientation

The location, orientation and strength of current sheets in 3D is vital for providing an environment for fast magnetic energy release. This section is concerned with investigating the buildup of current sheets in the various experiments, with the aim to study the relation between some basic model parameters and locations of reconnection.

As the emerging flux pushes its way into the coronal magnetic field, stress builds up at the interface between the two flux systems. When the two flux systems are antiparallel ( $\phi_0 = 180$ ), a current concentration is formed all over the emerging plasma hill. As the stress continues to build up the current is concentrated into a narrow curved sheet that reaches from the summit point of the plasma hill down its sides towards the photosphere almost along the direction of the underlying emerging flux tube in the  $y$ -direction. As the orientation of the coronal magnetic field changes in the different experiments, the orientation and strength of the current sheet changes too. The current sheet is found to rotate around its vertical central axis as a monotonic function of the angle  $\phi_0$  between the coronal magnetic field and the emerging magnetic field (see also Fig. 3), where  $\cos \phi_0 = (\mathbf{B}_{cor} \cdot \mathbf{B}_t) / |\mathbf{B}_{cor}| |\mathbf{B}_t|$ ,  $\mathbf{B}_t$  represents the tube field at the summit point of the emergence region.

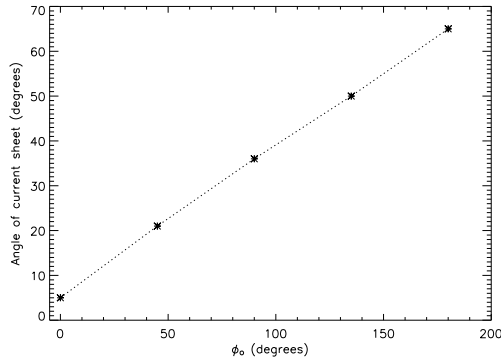


Fig. 3.— The orientation of the current sheet with respect to the vertical  $yz$  midplane as a function of the angle between the two magnetic flux systems.

The orientation of the current sheet can be found using the following analysis. Assume we are only interested in the orientation at the summit

point of the emergence, then the  $z$  component of the field can be ignored. In general, the field vectors can be expressed in terms of an orthogonal coordinate system, with one unit vector,  $\mathbf{e}_1$ , defined by the direction given by the sum of the magnetic vectors,  $\mathbf{B}_{cor} + \mathbf{B}_t$  and the other unit vector,  $\mathbf{e}_2$ , orthogonal to this defining a right hand system. Thus,

$$\mathbf{B}_{cor} = B_{cor\parallel} \mathbf{e}_1 + B_{cor\perp} \mathbf{e}_2, \quad (2)$$

$$\mathbf{B}_t = B_{t\parallel} \mathbf{e}_1 + B_{t\perp} \mathbf{e}_2 \quad (3)$$

The components of  $\mathbf{B}_{cor}$  and  $\mathbf{B}_t$  along  $\mathbf{e}_1$ , namely  $B_{cor\parallel}$  and  $B_{t\parallel}$ , represent the components of the magnetic field that cannot be annihilated and at the same time determine the direction of the main axis of the current sheet. The components along  $\mathbf{e}_2$ ,  $B_{cor\perp}$  and  $B_{t\perp}$ , provide two oppositely directed components that can annihilate in a reconnection process. The integrated current across the sheet is simply given by  $|B_{cor\perp}| + |B_{t\perp}|$ . Visualization of the current sheet and illustration of its orientation in the computational volume is shown in Section 6.

#### 3.1. Magnetic Pressure Balance Across the Current Sheet

In 2D the total pressure balance across a current sheet is simple, and it maintains a change between magnetic and gas pressure. In 3D such a balance may change with time as the relative orientation of the field that is advected into the sheet changes. In this paper, the evolution of the total pressure balance is used as an indirect indicator of magnetic reconnection.

As the tube rises the current sheet moves upward covering the upper part of the buoyant flux system. Archontis et al. (2005) showed that the magnetic pressure distribution across the current sheet changes with time in experiment A. This change in the temporal evolution of the magnetic pressure was found to play an important role in the reconnection process between the two flux systems.

Figure 4 shows the pressure of the horizontal component of the magnetic field ( $B_{hor}$ ) below (solid line,  $|\mathbf{B}_t|$ ) and above the current sheet (dot-dashed line,  $|\mathbf{B}_{cor}|$ ) as a function of time. The dashed line represents the pressure from the  $B_x$  component of the magnetic field below the current

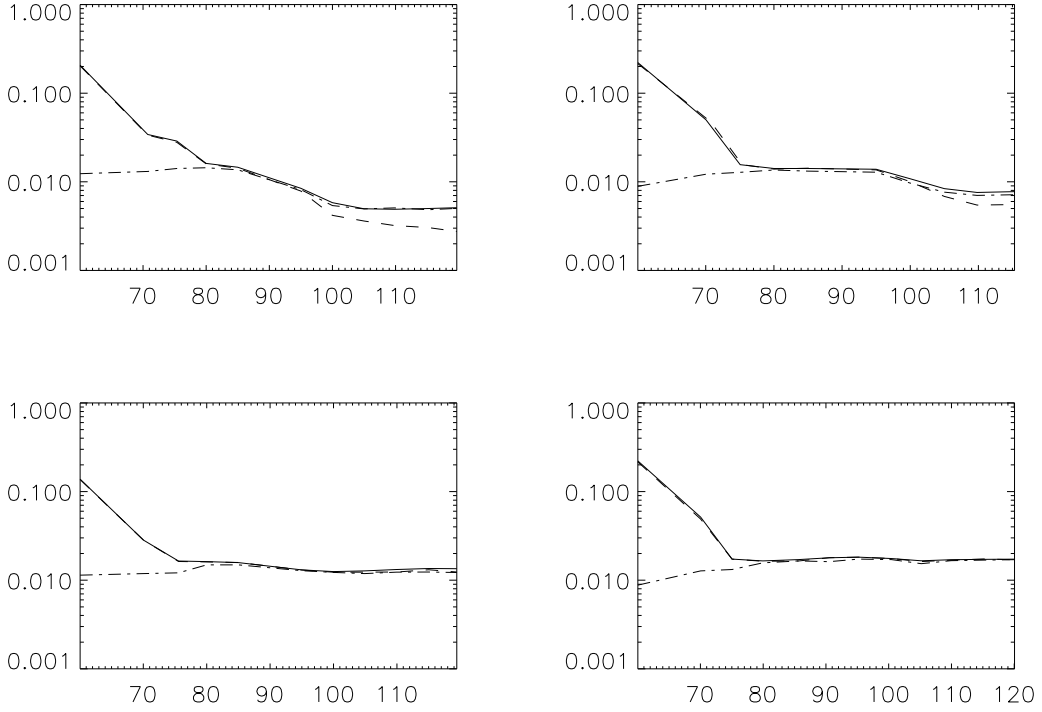


Fig. 4.— Temporal evolution of the magnetic pressure just above and below the current sheet are shown for experiments A, B, C and D from top-left to bottom-right panel. Full line represents the pressure below the sheet, the dot dashed line indicates the pressure above the sheet. Finally the dashed line indicate the pressure from the magnetic component perpendicular to the tube direction just below the sheet.

sheet.

At the beginning of the emergence process the magnetic pressure inside the rising plasma is much larger than that of the ambient coronal field. At  $t \approx 60$  the difference is more than one order of magnitude. This pressure excess pushes the emerging tube upwards into the atmosphere - for details see the discussion of forces given in Section 5.2. After  $t \approx 80$  a transverse balance of magnetic pressure is achieved, independently of the different orientation of the ambient field, and this balance remains until the end of the simulation.

Before  $t \approx 95$  the  $B_x$  and the  $B_{hor}$  of the rising magnetic field in the tube, are approximately equal. For experiments A and B the two components separate around this time, indicating that the orientation of the emerging magnetic field just

below the interface changes with time. The reason being that, as time proceeds, the uppermost field lines of the rising plasma reconnect with the ambient field and this allows for different internal flux layers to come into contact with the overlying flux system; the magnetic field vector in these internal layers points increasingly away from the transverse direction and this explains the decrease apparent in the dashed curve in experiments A and B. On the other hand, for experiment C and D the reconnection affects a much shallower region of the rising tube, and, as a result, the x-component of the field as the interface does not decrease.

Finally, it is found that pressure at the end of the experiments,  $t = 120$ , has an almost linear dependence on the value of  $\phi$ , providing the highest magnetic pressure for the cases that do not show effective reconnection in Fig. 4. The effects and importance of reconnection is further discussed be-

low.

#### 4. Magnetic Connectivity

In the previous section we showed that the emerging flux tube reconnects with the coronal magnetic field, at least for the cases A - C. As a result of this the magnetic pressure below the current sheet changes with the relative horizontal angle  $\phi_0$ . Thus, it seems plausible that the emergence process will be strongly influenced by the orientation of the coronal field. For example, when the two fields are approximately parallel one might expect the reconnection process to be slowed substantially and the emergence process possibly hindered. This section investigates the efficiency of reconnection, from a global point of view, by

- measuring the height of the apex and axis of the emerging tube in time (Section 4.1),
- measuring the amount of horizontal and normal flux that emerges into the corona (Section 4.2),
- studying the changes in field line connectivity (Section 4.3), and finally by
- measuring the fraction of the tube flux that reconnects in time (Section 4.4).

##### 4.1. Height-time relation: apex and axis

To measure the dependence of the rising motion of the tube on the orientation of the ambient field, we find the height of the apex and the axis of the rising tube as a function of time for the experiments listed in Table 1. More precisely, a large number of field lines are traced from starting points along the central vertical line. Then we find those fieldlines that stay in the tube and those that belong to the ambient magnetic field. The summit point is then the first point along the central line at which the connectivity changes.

Fig. 5 (left panel) shows the height-time relation of the apex and the center of the emerging tube. The emergence starts with a slow rise phase while the flux tube is below the photosphere (Murray et. al. (2006) investigate how this initial emergence phases depend on the tube parameters). This is followed by a rapid rise phase between  $t = 55$  and  $t = 80$  during which the apex

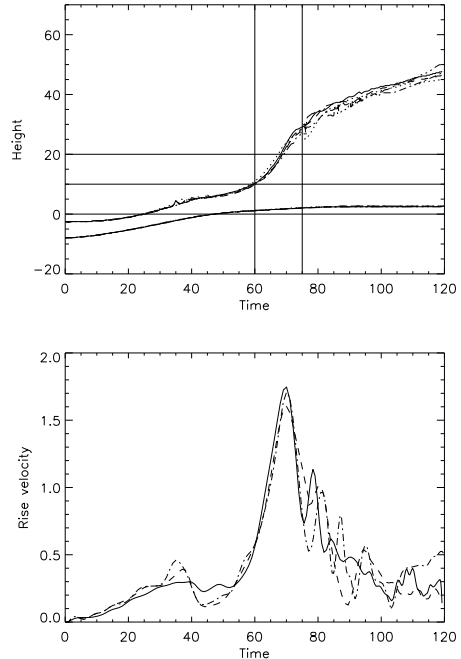


Fig. 5.— Left: The height of the apex (upper curves) and the center (lower curves) of the tube as a function of time. Right: The associated velocity of the apex of the rising system. For line styles see Table 1.

of the tube rises through the transition region and into the corona. After  $t = 80$  the rise rate slows down and settles down to a lower rate that fluctuates with time and between the various experiments, but on average follows the same trend. The change in the height-time relation around  $t = 75$  corresponds to the time at which magnetic pressure balance across the current sheet is achieved, as seen in Section 3.1. At this time the width of the current sheet shrinks to the numerical resolution limit.

The lower curves in the top panel of Figure 5 show that the axis of the tube reaches the photosphere at  $t \approx 45$  and remains close to the lower region of the photospheric layer until the end of the simulation. A similar result is found in previous experiments of flux emergence (Fan 2001; Magara & Longcope 2003; Archontis et al. 2004; Manchester et al. 2004).

Finally, the right panel of Fig. 5 shows the rise velocity of the apex of the tube. It is seen that

all experiments follow the same evolution until  $t \approx 75$ , after which a general decrease with superimposed oscillations are seen in the rise velocity.

#### 4.2. Emerging flux

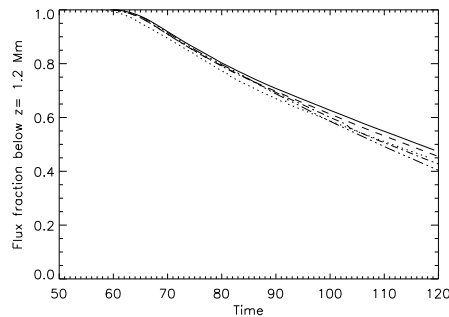


Fig. 6.— The graphs show the fraction of flux below  $z = 1.2$  Mm as a function of time for the five experiments mentioned in Table (1). Almost 65% of the flux has emerged into the corona at  $t=120$  for experiment A.

Another global measurement of the amount of the emerging flux in time can be obtained by calculating the amount of new horizontal flux passing through the vertical midplane ( $x$ - $z$  plane located at  $y = 0$ ) and above a height of  $z = 1.2$  Mm. This particular reference height is chosen to be above the initial flux tube and below the initial coronal magnetic field. In this way, the initial coronal flux, independent of its orientation, does not contribute to the measurement.

Alternatively, we can measure the amount of horizontal flux that remains below the height of  $z = 1.2$  Mm in time. This amount of flux is defined by:

$$\Phi(t) = \int_{-L_x}^{L_x} \int_{-L_z}^{1.2} B_y(x, 0, z, t) dz dx. \quad (4)$$

Fig. 6 shows  $\Phi(t)$ , normalized by its value at  $t = 0$ , as a function of time for the five experiments. The profiles for the five experiments are almost identical until  $t = 90$ . This result shows that the amount of flux that emerges into the upper atmosphere is almost independent of the relative horizontal angle,  $\phi_0$ . After  $t = 90$ , we find that the larger the initial angle,  $\phi_0$ , is between the emerging flux and

the coronal magnetic field, the larger is the fraction of the magnetic flux that emerges into the coronal regime at a given time. However, the difference in emerged flux between experiment A and experiment E is found to be small, close to 7%, at the end of the experiment, at which time about 60% of the initial flux has emerged into the outer atmosphere.

Observationally Kubo et al. (2003); Spadaro et al. (2004) and Zuccarello et al. (2005) have measured the development of the normal flux represented by the emerging region. They find a time dependent growth, that over the first few days is close to linear. This is followed by a saturation of flux and eventually a decrease. The grow rates of the magnetic flux in the three cases are naturally different. One striking difference with the numerical experiments is the time scale involved. In the observations the timescale of the evolution of the system is measured in days, while the experiment here only covers about 20 minutes. Therefore it will not be possible to make a real comparison, but it is interesting to compare the structure of the comparable numerical measurement of the emerged magnetic flux.

If one assumes the emerging region is at the disk center, then the observed quantity is equivalent to integrating the positive(/negative) flux represented by the  $B_z$  component in our experiments:

$$\Phi(t) = \int_{-L_x}^{L_x} \int_{-L_y}^{Ly} B_z(x, y, z, t) dy dx. \quad (5)$$

Fig. 7 shows the time evolution of the positive vertical flux through the transition region ( $z = 1.2$  Mm). The plot shows two different phases in the evolution: first a near linear increase of the vertical flux until about  $t = 75$ , followed by another phase with a continuously decreasing rate. The difference in the time evolution of the vertical flux between the different experiments is very small.

Despite significant differences in the timescales between observations and these experiments, the basic structure of the emerging flux appears very similar.

#### 4.3. Field line connectivity

The magnetic energy released in reconnection events is bound to spread along the reconnected

field lines due to anisotropic heat conduction. The bright structures found in EUV and X-ray observations in association with flux emergence, and other energy release events, are therefore providing vital information about the field line connectivity in the corona. Comparing the coronal structures with models provides us with a possibility of understanding the field line structure of dynamical events.

There are several ways to show, in a qualitative manner, how the fieldline connectivity changes in time for the various experiments. We choose to trace field lines starting from one end of the submerged tube and see if they either connect to the other end of the tube or to the corona. A disk is selected at the tube end, centered on the initial tube axis, and the destination of a large number of field lines is determined. Field lines going from the one end of the tube to the other are colored grey and field lines connecting to the corona are colored black. This method indicates the global connectivity of the fieldlines between the two flux systems. Details of the method can be found in Parnell et al. (2004).

Figure 8 consists of five columns. Each column corresponds to a different experiment and shows how the field lines, which have been traced from inside the selected disk, change their connectivity in time. The left column, for example, shows the connectivity for experiment A. The four panels in the left column show that the connectivity changes first at the outer layer of the disk and then moves toward the center following a swirling

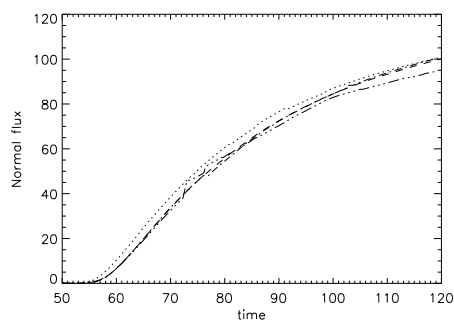


Fig. 7.— Time evolution of the normal flux of the emergence through the  $z = 1.2$  Mm plane for the five experiments. For line styles see Table (1).

motion. This is because the fieldlines which are traced from the outer periphery of the disk, reach higher levels in the atmosphere and reconnect first with the ambient field. At the end of the simulation only few fieldlines, which are found in a short distance around the center of the disk, have not changed connectivity yet. All the other fieldlines have already been reconnected with the ambient field.

We also find that at each time the number of fieldlines that do not change connectivity is smaller, as the relative horizontal angle between the two flux systems increases from  $\phi_0 = 0$  (right column) to  $\phi_0 = 180$  (left column). As a result, there are very few fieldlines that have been reconnected at the end of the simulation for experiment E, whereas most of the fieldlines inside the disk have change their connectivity in experiment A.

It has to be noticed that the disk used for tracing the field lines is not changed in time, implying that the starting points do not represent exactly the same footpoints in time. Investigating the drift velocity of the flux pattern it is found to be far to small to account for the change in connectivity between  $t = 60$  and  $t = 80$ . A closer examination of the field line structure shows that field lines at the top of the reconnection sheet continuesly changes connectivity (as shown in Archontis et al. (2005)), being slowly pushed towards the flanks of the diffusion sheet. Here they re close and again become part of the flux tube. In other words, flux from footpoints at side of the emerging flux region is involved in reconnection processes more than ones already in the early phase of the emerging process.

#### 4.4. Flux connectivity

To further illustrate the results obtained in the previous section, we calculate the amount of flux that remains in the tube and does not reconnect, normalized to the total flux within the disk, as a function of time.

$$\Phi(t) = \frac{\int_{\text{black area}} B_y(x, l, z, t) dx dz}{\int_{\text{disk}} B_y(x, l, z, t) dx dz}. \quad (6)$$

$\Phi(t)$  is shown in the top panel of Fig. 9 for the five experiments in Table (1).

Flux emergence through the photosphere starts at around  $t = 60$  and reconnection between the two flux systems starts shortly after this for most

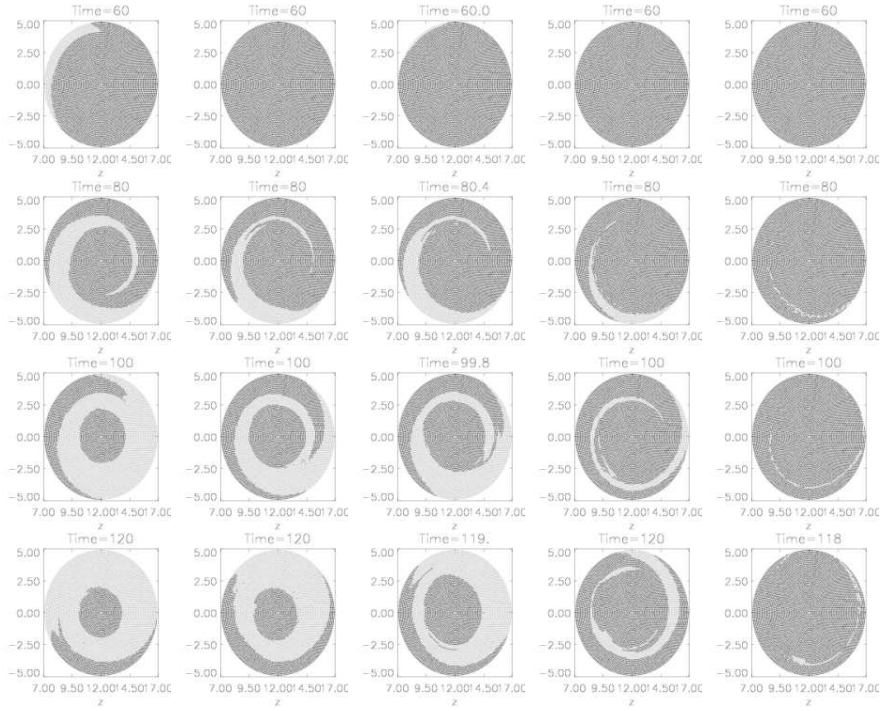


Fig. 8.— Connectivity plots for the five experiments. The five columns represent the A, B, C, D and E case respectively. The rows show the connectivity at times close to 60, 80, 100 and 120. The disks show the area in the tube at the  $y$ -boundary from where the fieldlines are initially traced.

of the experiments. A measure of the reconnection rate is given by the absolute value of the slope of the lines in the left frame of Fig. 9. This shows that there is a short initial phase where the reconnection rate builds up, followed by a period of time where the reconnection proceeds with different, but almost constant, rates in all experiments. After  $t \approx 100$  the reconnection rate decreases for the three fastest reconnecting experiments, to a lower level that is roughly maintained until the end of the experiments. The reconnection rates are simply given by the gradient of the connected flux fraction. As already stated earlier, an unknown amount of flux reconnects more than once, implying that global-double-separator bifurcations may take place, Haynes et al. (2006), through which recycling of the flux may occur, Paranell et al. (2006). The estimates of the reconnection rate are, therefore, only providing a minimum value and cannot be used, to estimate the reconnection speed in the reconnection processes. This implies that a quantitative comparison with Longcope et al. (2005) results is not pos-

sible. Longcope et al. (2005) used TRACE and MDI observations to estimate the energy transfer between a new emerging region and old coronal magnetic field. Their results showed that reconnection was not active for a long initial phase, after which a large fraction of the emerging flux connected to the coronal field over a relative short timescale. In our simulations, we find a more smooth increase in the flux interaction, with a clear leveling off towards the end of the experiment. Hidden in this may well be a significant restructuring of the field that is not apparent due to limitations in following the connectivity of individual flux concentrations.

Despite this, the graphs still provide information about the general development of the experiments. The right frame of Fig. 9 indicates that experiment A has the highest rate of reconnection and that the reconnection rate decreases as the angle between the two flux systems becomes less favorable and the magnitude of the reconnecting field component decreases. This fact is unlikely

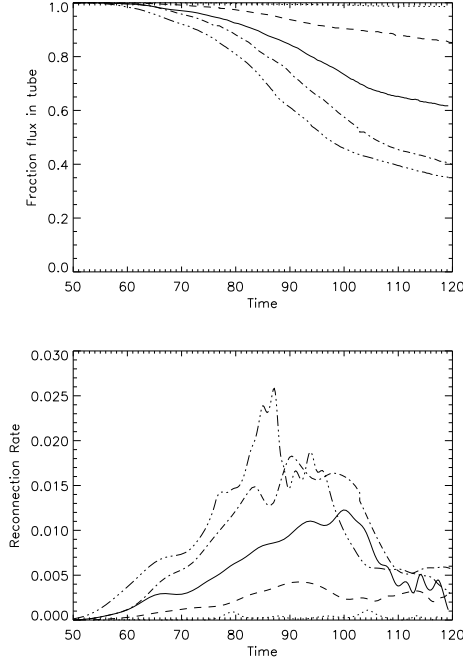


Fig. 9.— The left panel shows how the flux connectivity, as defined in Eq. (6), changes with time for the different experiments. The right panel represents the reconnection rate of the experiments by simply estimating the gradient of the curves in the left panel. The line style is given in Table 1.

to be changed since the multiple reconnection depends on field lines already having changed connectivity once. Thus, the amount of reconnected flux in experiment A increases up to 65% by the end of the simulation while it remains close to zero when the two flux systems are parallel. Finally, we find that the amount of flux that remains in the tube at the end of the experiments ( $t=120$ ) decreases nearly as  $1 - 0.65 \sin(\phi_0/2)$ . In other words, it scales with the orientation, and therefore the strength, of the current sheet.

## 5. Dynamics of emergence

In the previous section we showed that the height-time relation of the apex of the tube is similar in all experiments. It is also found that the amount of flux that emerges through a certain height as a function of time does not depend on the orientation of the ambient field. However, the

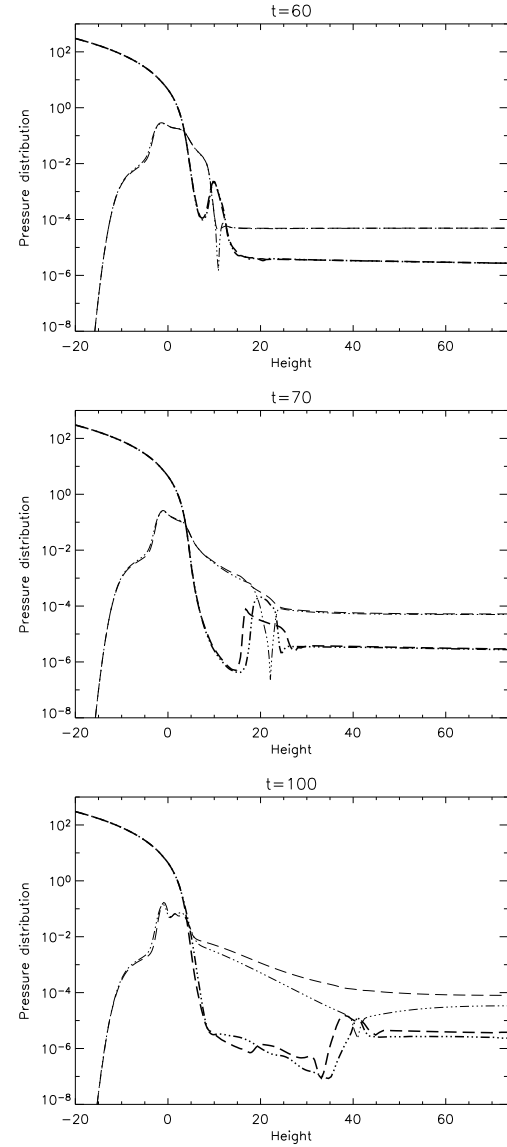


Fig. 10.— Magnetic pressure (thin lines) and gas pressure (thick lines) distribution along height for the experiments A and D along the central vertical line. Line style are given in Table (1)

amount of flux that changes connectivity between the emerging flux and the coronal magnetic field, depends critically on the relative orientation of the two flux systems.

In the experiments where the rate of change of connectivity is high, the overlying coronal magnetic field is constantly removed by the reconnec-

tion process. Thus, the volume above the rising tube is opened and the buoyant system can make its way up into the upper atmosphere. On the other hand, in the experiments with very little reconnection, the coronal magnetic field is not easily removed but instead is pushed upwards and keeps up resistance to the rising motion of the tube (the fieldline topology at the top part of the emerging tube is illustrated in Section 6). Thus, one may ask why the rising motion of the tube is not influenced by the change of connectivity in the different experiments.

In fact, the height-time relation of the apex of the tube indicates that the process of flux emergence is predominantly governed by the dynamics of the rising magnetized plasma. Thus, in the following sections, first we consider the gas and magnetic pressure distribution along height, inside the expanding rising volume and across the current sheet, for two experiments with different initial relative angle (Section 5.1); then we study the temporal evolution of forces that act on the upper part of the buoyant tube (Section 5.2).

### 5.1. Pressure distribution

It has been shown, (Fig.5 in Archontis et al. (2005)), that the three-dimensional current sheet which is formed between the two flux systems in experiment A, is the location of a rapid change in the direction of the magnetic field. In the early phase of the evolution of the system the total magnetic field vector goes through a tangential discontinuity across the current sheet with a clear minimum at the center of the sheet. As time proceeds the direction of the field changes smoothly across the interface of the two flux systems following a rotational-like discontinuity.

Figure 10 shows the gas pressure and magnetic pressure along the central vertical line for the experiments A and D at  $t = 60, 70$  and  $100$ . The first panel of Fig. 10 ( $t = 60$ ) shows that in both experiments the magnetic pressure is higher than the gas pressure inside the expanding volume ( $5 < z < 10$ ) by almost two orders of magnitude. The plasma  $\beta$  in this region is therefore very low. The magnetic pressure decreases across the interface between the two flux systems and has a minimum value inside the current sheet. This is most easily seen in the top left panel of Fig. 10 for the triple dotted dashed line. This position corre-

sponds to the pronounced minimum of the magnetic pressure occurring at the position of maximum electric current, that is due to the tangential discontinuity across the sheet. At the same time the total pressure has a smooth change over the current sheet. This implies that the plasma  $\beta$  increases in the current sheet and becomes larger than unity. At this early stage of the experiment reconnection at the top of the rising tube has not started yet and thus the pressure distribution is almost identical in the two experiments.

The top right panel of Fig. 10 shows the pressure distribution when reconnection occurs between the tube and the ambient field. In experiment A, the magnetic pressure still goes through a sharp minimum, although the value of the minimum is higher than at  $t=60$ . In experiment D, instead, then magnetic pressure has a smooth distribution across the interface, with no minimum. In either case, the gas pressure supplements the magnetic pressure across the interface, so that the total pressure distribution has no extrema here. The reason for the different behavior of the magnetic pressure profiles for the two experiments is the presence of an important non-zero, non-reconnecting field component in the current sheet in experiment D which is nearly absent in experiment A.

Finally, the bottom panel shows the distribution at a later time, at  $t = 100$ . Now, the direction of the total magnetic field vector in experiment A changes smoothly across the current sheet following a highly compressed rotational discontinuity. Thus, there is a finite non-reconnecting magnetic component in the current sheet and the magnetic pressure there becomes higher compared to the magnetic pressure at  $t = 70$ . The gas pressure in the top of the rising system has decreased because the dense plasma which was carried upwards has been reconnected. In experiment D, the gas pressure and the magnetic pressure do not change dramatically compared to the same distribution at earlier times. Thus, the magnetic pressure inside the expanding volume in experiment D now is much higher than the magnetic pressure in experiment A. At all times, the magnetic pressure exceeds the gas pressure and dense material is lifted up against gravity.

By looking at the pressure profiles with height in the bottom panel of Fig. 10, one notice that

in experiments A the current sheet region experiences a pressure minimum. This is a consequence of the Bernoulli effect associated with the lateral emission of reconnection outflows from the diffusion region: the gas pressure depletion in the region helps accelerating the plasma from above and below into the the current sheet, thereby bringing new magnetic flux in to the reconnection site.

From these plots it is also found that the total pressure increases with time in experiment D. This is a pileup effect as the upper boundary is closed and, thus, the growing excess pressure cannot propagate through the top boundary.

## 5.2. Forces

In this section, we focus our attention on the forces that act on the upper part of the expanding rising volume, just below the current sheet. In the following, we consider experiment A.

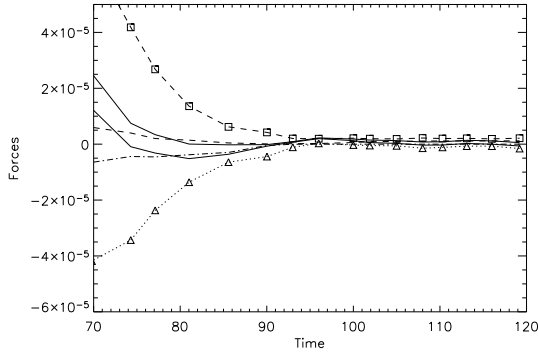


Fig. 11.— Temporal evolution of the vertical forces acting below the current sheet along the  $(x = 0, y = 0)$  line. Shown are the magnetic pressure gradient (dashed-rectangles), the tension force (dotted-triangles), the gravitational force (dotted-dashed), the Lorentz force (solid), the gas pressure gradient (dashed) and the total force (thick solid).

The vertical component of the forces is shown as a function of time in Fig. 11. The plot shows that the emergence of the buoyant tube is driven by the magnetic pressure force that exceeds all the other forces at the early stage of the evolution. What is also noticeable is that the magnetic pressure force and the magnetic tension are equal in magnitude and opposite in sign and that they are substan-

tially larger than either the pressure gradient or the gravity force.

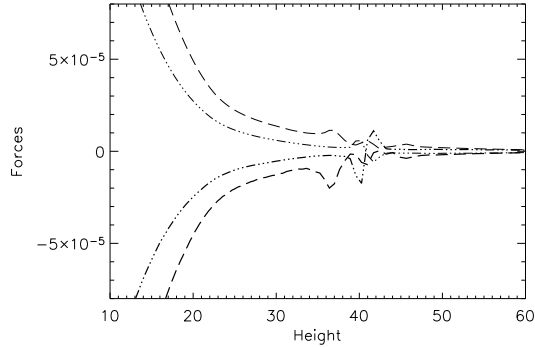


Fig. 12.— The variation of the magnetic pressure force (thin lines) and tension force (thick lines) with height for experiment A (triple dotted dashed lines) and D (dashed lines) at  $t = 100$ .

The total force is clearly positive accelerating the emerging field against gravity until  $t \approx 72$ . This is followed by a short period of deceleration. After  $t = 95$ , all the forces become very small and are essentially in balance. This result is consistent with the motion of the plasma, which rises with an almost constant velocity after  $t = 95$  (see right panel in Fig. 5). Notice that the temporal evolution of the total force corresponds well with the motion of the apex of the tube shown in Fig. 5. Also, the time ( $t = 95$ ) at which the forces take on very small values corresponds to the time at which pressure balance is achieved across the current sheet.

An analysis of the forces for the experiments B-D show that the temporal evolution of the total acceleration is similar to the experiment A. This result explains why the apex of the tube reaches almost the same height at the same time in all experiments. To further illustrate the point made above we examine the total force for the experiments A and D for  $t = 100$ . The  $z$ -component of the total force is

$$F_z = F_{l_z} + F_g + F_p, \quad (7)$$

where  $F_g = -\rho g$  is the gravitational force,  $F_p = -\frac{\partial P}{\partial z}$  is the gas pressure force and  $F_{l_z}$  is the vertical component of the Lorentz force. The latter is

written as

$$F_{l_z} = \frac{1}{4\pi} (\mathbf{B} \cdot \nabla) B_z - \frac{1}{8\pi} \frac{\partial B^2}{\partial z}, \quad (8)$$

where the first term describes the magnetic tension and gives a force when the fieldlines are curved, while the second term is the magnetic pressure force that acts from regions of high magnetic pressure to regions of low magnetic pressure.

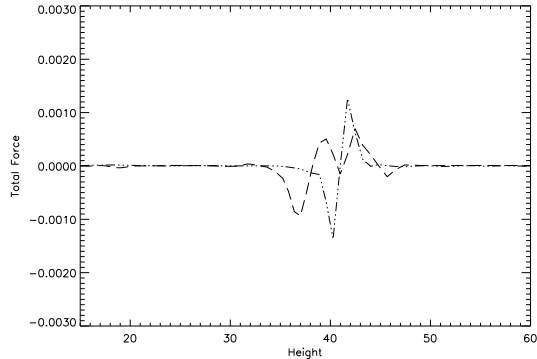


Fig. 13.— Total force as a function of height for experiment A (triple dotted dashed line) and D (dashed) at  $t = 100$ .

Fig. 12 shows the distribution of the two terms in Eq. (8) along height for the experiments A and D for  $t = 100$ . On the one hand, the vertical component of the magnetic pressure force below the current sheet ( $z < 40$ ) is larger for experiment D. On the other hand, the tension force, which is a downward force, is also larger for experiment D and, thus, the Lorentz force has comparable size in both experiments.

Finally, Fig. 13 shows the distribution of the total force in Eq. (7) along height for the experiments A and D for  $t = 100$ . The total force at the top part of the rising flux system is very small and almost identical for A and D. Thus, it seems that the total acceleration that acts on the expanding rising volume below the current sheet does not depend on the structure of the overlying field and as a result the crest of the tube reaches almost the same height at the same time for experiments with different orientation of the coronal field.

## 6. Topology of the emerging region and magnetic reconnection

The topology of the interacting magnetic field is important for understanding the structure of the emerging high velocity jets and associated hotter plasma distribution. In this section, we show how different is the structure of the magnetic field that appears in the corona when the relative orientation of the interacting magnetic fields changes between the experiments.

The three-dimensional geometry of the current sheet and the jets, emanating from the rims of the current sheet, for experiment A and B, have been studied by Archontis et al. (2005) and Galsgaard et al. (2005). Here, we illustrate the projection on horizontal  $xy$  planes of the three-dimensional structure of the sheet for experiments A-E. Fig. 14 shows five panels containing colourmaps of the total magnitude of the current ( $|J|$ ) on a horizontal cut at a height of 1.7 Mm above the base of the corona at  $t = 100$ . The arrows in the panels correspond to the projection of the velocity field.

The bright patches in Fig. 14, show the location of the highest values of  $|J|$ , and correspond to the intersection of the horizontal cut with the arch-like current sheet. Effective reconnection occurs and high-velocity outflows are ejected sideways from these sites. The velocities of the jets reach values close to  $200 \text{ Km sec}^{-1}$  in experiment A and B. In experiments A-D, the direction of the jets is aligned with the direction of the ambient magnetic field. In experiment E there are no jets because reconnection does not occur actively between the two flux systems. The arrows in this case illustrate the drain of the plasma from the uppermost layers of the emerging plasma ball as it rises and pushes the ambient field upward.

The weaker current structure, forming an enclosure between the two locations of strong current, outlines the border region between the magnetic flux totally connected to the emerging flux tube (inside) and either the reconnected flux or the original coronal flux (outside). From this it is clear that the horizontal volume of the emerging flux tube decreases significantly as reconnection becomes more favorably. It is only the flux contained inside this volume that eventually can end up outlining the structure of the emerging flux re-

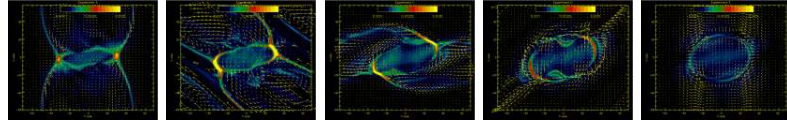


Fig. 14.— Colourmaps of the total current at  $t = 100$ . Superimposed is the velocity field (arrows). The panels correspond to the experiments A-E.

gion, while the reconnected field lines connect the two flux concentrations to neighboring flux regions (here only the corona).

To further illustrate how the three-dimensional reconnection works at the top of the emerging flux system we study the topology of the fieldlines across the current sheet at  $t = 100$ . Figures 15 and 16 consist of ten panels that show the fieldline topology for the five experiments. Three sets of fieldlines have been traced from different starting positions along height and across the interface of the two flux systems close to the center of the emerging region. The blue fieldlines are traced from just below the current sheet and belong entirely to the rising tube. The red fieldlines are traced from just above the sheet and are ambient fieldlines. Finally, the yellow fieldlines are traced from inside the diffusion region and connect the tube with the coronal field. The current concentration at the interface is visualized with a transparent isosurface.

The general picture of the reconnection shows a clear difference from the traditional two-dimensional configuration. This is because the magnetic field vector across the sheet resembles a rotational discontinuity. On the one hand, the uppermost rising fieldlines have an orientation which is not perfectly aligned with the  $x$ -axis, as has been explained in Archontis et al. (2005). On the other hand, the orientation of the ambient fieldlines changes from experiment A to experiment E so that the relative horizontal angle between the two systems increases. The product of the reconnection between these two sets of fieldlines is another set of fieldlines, the yellow lines, which are ejected sideways from the current sheet and establish links between the solar interior and the outer atmosphere. Panels B2, C2 and D2 show that the yellow fieldlines at the top of the current sheet have an intermediate orientation between the blue and the red fieldlines and that they do not stay in a two-dimensional plane but they experience

full 3D-reconnection. The only experiment where the initial relative orientation is not favorable for reconnection is experiment E. Panels E1 and E2 show that there is no reconnection (and thus, no yellow fieldlines in the panels). Instead, the coronal field is pushed upwards and a bended hill-like shape interface is formed between the two fields. At the late stages of the evolution of the system the ambient field slides down along the sides of the hill of the emerging flux and some reconnection occurs at low heights.

Through figures 15 and 16 we also get a confirmation of the dependence of the volume of the emerged region on the orientation of the coronal field that are shown in Fig. 14. More precisely, the blue fieldlines illustrate the geometry of the outermost layers of the tube and show that the expansion, in the transverse direction to the axis of the tube, is larger when reconnection is less efficient. Indeed, in the case of experiment A the outer fieldlines that suffer a large expansion reconnect first and as the time goes on more internal layers, which expand less and are also less twisted, come into contact and eventually reconnect with the ambient field. In contrast to this, experiment E shows a large expansion of the loops of the upper fieldlines as these have not been reconnected due to the small angle  $\phi_0$ . This picture confirms the indications regarding the location of the current structure seen in Fig. 14.

Finally, if we focus on the shape of the emerging fieldlines we find that the blue lines in experiment A represent fieldlines which were initially located closer to the main axis of the tube and their orientation was not far away from the  $y$ -axis. When these fieldlines emerge (see Panel A1 and A2) keep an almost flat shape in the middle of their crest. On the other hand, the outermost fieldlines in experiments with less reconnection (see for example the panels E1 and E2) represent fieldlines which were initially located at the outskirts of the tube and they had larger curvature. As these fieldlines

rise and expand, they keep their convex shape and, thus, the magnetic tension force at the top of the emerging tube becomes larger compared to the experiments with more efficient reconnection. In fact, this has been also shown in Fig. 12, where the magnetic tension is plotted against height for the experiments A and D at  $t = 100$ .

## 7. Discussion

The present experiments were terminated at around  $t=120$  due the use of periodic boundary conditions in the horizontal direction. For times after  $t=120$  the effect of these conditions become very apparent on the experiments as the reconnection jets have propagated across the system, and the subsequent evolution is not showing a freely expanding magnetic flux concentration. In the Sun, this scenario is possibly more realistic, than having open boundary conditions. On the other hand, it may cause numerical problems and influences the dynamical evolution of the system. Thus the timescale of each numerical experiment depends also on the boundary effects from the periodic conditions.

Some observations seem to favor a situation where a flux rope is emerging into the corona as coherent structure (Lites et al. 1995), while others (Strouse & Zwaan 1999; Pariat et al. 2004) indicate a pattern where undulating field lines make different dynamical effects to release the dense material in the lower parts along them. In our simulations, including our previous 3D numerical experiments, the initial flux tube becomes unstable to further expansion into the corona, by building up a dominating magnetic pressure force, due to the buoyancy of the tube (Archontis et al. 2004). When the force becomes strong enough it "blows" the layers close to the transition region up and into the corona, where they rapidly push the overlaying material away and created a dense, cold magnetically dominated plasma dome. These experiments show that almost 65% of the normal flux of the initial flux tube has emerged into the corona. We also find that the axis of the initial tube has not fully emerged yet above the photosphere. It is worthwhile mentioning that in one of the experiments we find the formation of a horizontal current sheet, first reported by Manchester et al. (2004), which drives internal reconnection of the

flux belonging to the emerging tube, allowing the lower parts of the emerging flux tube to disconnect from the emerging flux system. This provides a mechanism to decouple the dense photospheric plasma from the field lines that expand into the corona (as indicated by Strouse & Zwaan (1999) and Pariat et al. (2004)) and provides a possibility for forming a structure that looks like an emerged twisted flux tube without emerging the entire magnetic flux system.

As it is seen from the Sections above, the relative orientation between the emerging magnetic flux and the coronal magnetic field is of great importance when it comes to the dynamical evolution of the flux interaction. The emergence process, eventually, produces high velocity plasma jets with temperatures in excess of average coronal values only in the cases of efficient reconnection. In less favorable situations the plasma will not be heated much and the spectacular display often seen in TRACE movies will not take place. Thus, the emergence of an easily observed flux region into the hostile coronal environment depends on a relative narrow span of angles between the two systems. On the Sun, this regime may be increased compared to the simple model presented here, due to the much larger structural complexity of the solar environment.

The experiments discussed here relay strongly to the evolution of driven magnetic reconnection. From analytical investigations of 2D reconnection (see Priest & Forbes (2000) and references there in), it is found that steady state reconnection depends critically on the structure of the magnetic field, the velocity flow and the value of the magnetic resistivity. This makes it natural to expect similar dependences to be carry over to steady state 3D reconnection. In relation to this, it is obvious that 3D numerical experiments are not able to resolve the Reynolds numbers present in the coronal plasma. Why should it then be expected that the results from the above mentioned experiments represent an evolution that may take place in the solar corona? Using hyperdiffusion the smallest length scale (the thickness) of the current sheet is alway only resolved by a few grid points, and it is only at these length scales that diffusion of the magnetic field becomes important. Increasing the numerical resolution, implies a decrease of the thickness of the current sheet

and through this a slight delay in the time for the initiation of reconnection. In the driven reconnection scenario presented here, the largescale of the magnetic field and velocity flow does not change significantly when the numerical resolution is increased and, thus, the magnetic flux advected into the current sheet will remain approximately the same. This indicates that magnetic reconnection provides the same new classes of connectivity. What may change is the local structure of the process, where increased numerical resolution can allow for reaching local turbulence in the current sheet as it may become tearing unstable before starting reconnecting. Such a process naturally makes it possible to reach a more complicated field line connectivity locally, but it also implies that the reconnection process becomes independent of the magnetic resistivity and responds directly to the amount of flux advected into the current sheet (Galsgaard & Nordlund (1996); Hendrix et al. (1996); Eyink & Aluie (2006)). Finally, the choise of resolution for the experiments is important. Experiments with low resolution yield low values for the energy release obtained in the simulations and large values for the timescale of the evolution of the system. High resolution, especially for the volume occupied by the initial tube, may cause problems with the entropy distribution and affect the buoyancy of the rising tube.

If the assumption of an emerging magnetic loop is correct, and the processes described in this paper and in our previous work are representative of the emergence of flux from the solar interior to the outer atmosphere of the Sun, then there are some simple features that this model may predict.

- The process of flux emergence is usually observed using vector magnetograms, which show the appearance of bipolar structures at the photosphere. In our experiments, due to the highly twisted magnetic flux tube in the subphotospheric layer, the orientation of the polarity patterns are, in the early phases, perpendicular to the main axis of the emerging flux tube (North-South orientation). As time progresses the two opposite polarity spots moving apart in the direction along the main tube axis (East-West orientation).
- The picture of an emerging bipolar region with its strong flux region located along the

axis of the main tube is only true for the photospheric layer during the short time of these experiments. Slightly above the photosphere the topology changes and the initial large scale bipolar region structure going across the magnetic loop is maintained over the remaining time of the various experiments. Variations between the different experiments are seen, but the systematic bipolar patterns going across the main axis of the initial flux tube is maintained for all experiments even for a height that is only 3400 Km above the photosphere.

- Magnetic reconnection between the emerging and coronal magnetic fields depends on the relative orientation between the two flux systems. Significant plasma heating and high velocity jets will appear when efficient reconnection occurs between the two flux systems in a coronal environment. For the cases where the relative orientation of the two flux systems is close to parallel, a weaker reconnection may take place closer to the photosphere.
- The emergence rate seems to depend on the structure of the magnetic field below the photosphere, which in our experiments has higher field strength than the coronal magnetic field. The excess magnetic pressure therefore expels the flux upwards and, thus, opens the volume for a new bipolar structure to appear.

The intense reconnection in the near anti-parallel cases makes it possible for most of the initial flux of the tube to reconnect with the coronal magnetic field. If this process continues for long enough, then the initial connectivity of the flux tube will be totally disrupted. It is therefore possible that by emerging a bipolar region into the hostile coronal environment, that the initial connectivity between the two opposite flux concentrations will be, at the least partly, disrupted. How severe this change in connectivity becomes depends on several factors, such as the structure of the coronal flux, the amount of the emerging flux and the duration of the reconnection process. A first estimate of the changes in the connectivity may be obtained simply by using potential models. On the other hand, it seems that these

models is not always the best method to follow for the study of the time evolution of magnetic structures in actively evolving regions, which is why we have not used this analysis here.

Further up in the atmosphere Longcope et al. (2005) have analyzed an interesting emergence observation recorded by TRACE. They adopt the minimum current model to estimate how much flux has reconnected. Using various assumptions they find it is possible to account accurately for the changes in connectivity. They also find that the reconnection between the emerging region and the existing coronal flux happens only after some time. As the interaction starts, it reaches a high activity level that last for a finite time before rapidly leveling off again. As most of the involved flux seems to be accounted for, then it indicates that the system has to build up a significant amount of stress before they start interacting. A different possibility is that the lower lying magnetic field structures are not favorable for the reconnection process and that the onset of the reconnection process does not start until some of the aligned flux has been pushed away and the relative orientation between the two flux systems has changed. It is also a possibility that the initial weaker reconnection process takes place in regions where the plasma density is still so high that the released dissipation can not heat the plasma to coronal temperatures. Finally there is the possibility that the initial coronal field in the emergence region is so weak that it does not provide for any significant heating as the new flux pushes its way up.

## 8. Summary

The emergence of new magnetic flux into an existing coronal magnetic field can evolve in very different ways. The coronal reaction on the emergence depends strongly on the relative orientation of the two flux systems. Efficient reconnection takes place only in the case where the two flux systems have almost antiparallel orientations. Taking place in the corona, this provides a number of very clear signatures, such as, high velocity jets and intense heating. The active reconnection process clearly affects the volume occupied by the magnetic flux totally connected with the underlying magnetic flux tube.

The reconnection between the two flux systems

can slow down mainly because of two reasons; Either because all flux in the emerging flux tube has reconnected with the coronal field, and by this totally disrupted the structure of the emerging flux rope. Or because the emerging process stops and the two flux systems find a mutual balance with each other where no, immediate, reconnection is taking place. Thus, the length and final structure of the new coronal magnetic field strongly depends on the total amount of emerging flux, its ability to reconnect and on the amount of the coronal magnetic flux.

For situations where the two flux systems are nearly aligned, it will be possible for the emerging field to penetrate far into the coronal magnetic field before it will create any significant coronal signatures revealing its present. These situations will only be easily spotted if simultaneous observations are made in photospheric and transition region lines.

In our simulations, we have used a simple energy equation that does not take into account optical thin radiation or anisotropic heat conduction in the corona. These effects are important ingredient to include in the experiments before more detailed comparisons with observations can be obtained. These are effects that will be discussed in future publication.

In a subsequent paper we are going to discuss in detail the local implications of the ongoing magnetic reconnection process and its implication on the dynamical evolution of the different experiments.

We are grateful for computational time on the UKMHD linux cluster in St. Andrews (Scotland, UK), funded by SRIF and PPARC, and on the linux cluster at the IAC (Tenerife, Spain) partially funded by the Ministry of Science and Technology. This work has also benefited from financial support through the *Platon* European Research Training Network HPRN-CT-2000-00153 of the European Commission and the CICYT project no. AYA2001-1649 of the Spanish Ministry of Science and Technology. K.G. was supported by the Carlsberg Foundation in the form of a fellowship. FMI thankfully acknowledges the computer resources, technical expertise and assistance provided by the Barcelona Supercomputing Center - Centro Nacional de Supercomputación (Spain) We

thank the anonymous referee for helpful comments that improved this paper.

## REFERENCES

Archontis, V., Moreno-Insertis, F., Galsgaard, K., Hood, A. & O'Shea, E. 2004, *Astron Astrophys*, 426, 1047

Archontis, V., Moreno-Insertis, F., Galsgaard, K., & Hood, A. 2005, *ApJ*, 635, 1299

Archontis, V., Moreno-Insertis, F., Galsgaard, K., & Hood, A. 2006, *ApJ*, 645, 161

Eyink, G. L. & Aluie H. 2006, *Physica D*, 223, 82

Fan, Y. 2001, *ApJ*, 554, L111

Fan, Y. & Gibson, S. E. 2004, *ApJ*, 609, 1123

Galsgaard, K., Moreno-Insertis, F., Archontis, V., & Hood, A. 2005, *ApJ*, 618, 153

Galsgaard, K. & Nordlund, A. 1996, *JGR*, 101, 13445

Georgoulis, M. K., Rust, D. M., Bernasconi, P. N. & Schmieder B., 2002, *ApJ*, 577, 506

Haynes, A., Parnell, C. E., Galsgaard, K. & Prist, E. R. 2007 *Proc. Roy. Soc. Lond. A Math. Phys. Eng. Sci.*, 463, 1097

Hendrix, D. L., Van Hoven, G., Mikić Z. & Schnack, D. D. 1996, *ApJ*, 470, 1192

Isobe, H., Miyagoshi, T., Shibata, K., & Yokoyama, T. 2005, *Nature*, 434, 478

Kubo, M., Shimizu, T. & Lites, B. W., 2003, *ApJ*, 595, 465

Leake, J. E. & Arber, T. 2006, *A&A*, 450, 805

Lites, B. W., 2005, *ApJ*, 622, 1275

Lites, B. W., Low, B. C., Martínez Pillet, V., Seagraves, P., Skumanich, A., Frank, Z. A., Shine, R. A. & Tsuneta, S., 1995, *ApJ*, 446, 877

Lites, B. W., Skumanich, A. & Martínez Pillet, V., 1998, *A&A*, 333, 1053

Longcope, D. W., McKenzie, D. E. , Cirtain, J. & Scott, J. 2005, *ApJ*, 630, 596

Magara, T. 2006, *ApJ*, 653, 1499

Magara, T. & Longcope, D. W. 2003, *ApJ*, 586, 630

Manchester, W., Gombosi, T., DeZeeuw, D., & Fan, Y. 2004, *ApJ*, 610, 588

Murray, M.J., Hood, A., Moreno-Insertis, F., Galsgaard, K., & Archontis V. 2006, *A&A*, submitted

Nordlund, Å. & Galsgaard, K. 1997, <http://www.astro.ku.dk/~kg>

Pariat, E., Aulanier, G., Schmieder, B., Georgoulis, M.K., Rust, D.M. & Bernasconi, P.N. 2004, *ApJ*, 614, 1099

Parnell, C., & Galsgaard, K. 2004, *A&A*, 428, 596

Parnell, C. E., Haynes, A. & Galsgaard, K. 2007, In Preperation

Priest, E. R. & Forbes, T. 2000, *Magnetic Reconnection*, Cambridge University Press

Spadaro, D., Billotta, S., Contarino, L., Romano, P. & Zuccarello, F. 2004, *A&A*, 425, 309

Strouse, L. H. & Zwaan C., 1999, *ApJ*, 527, 435

Zuccarello, F., Battiato, V., Contarino, L., Romano, P., Spadaro, D. & Vlahos, L. 2005, *A&A*, 442, 661

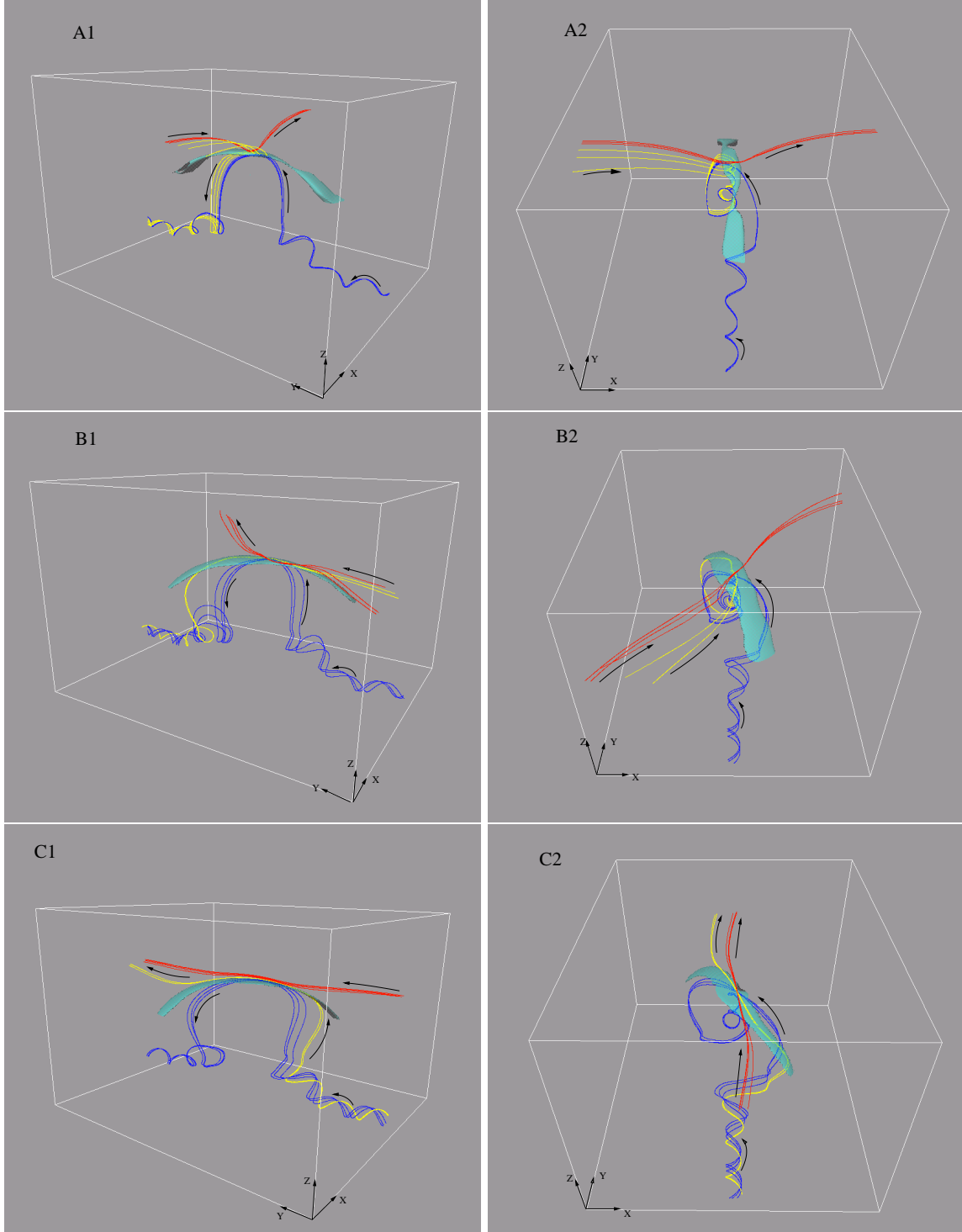


Fig. 15.— 3D visualization of the fieldline topology across the current sheet at  $t = 100$  for the experiments A (panels A1, A2), B (panels B1, B2) and C (panels C1, C2). The left column is a side view and the right column is a top view of the same snapshot. The current sheet is visualized as transparent isosurface. The arrows show the direction of the magnetic field vector.

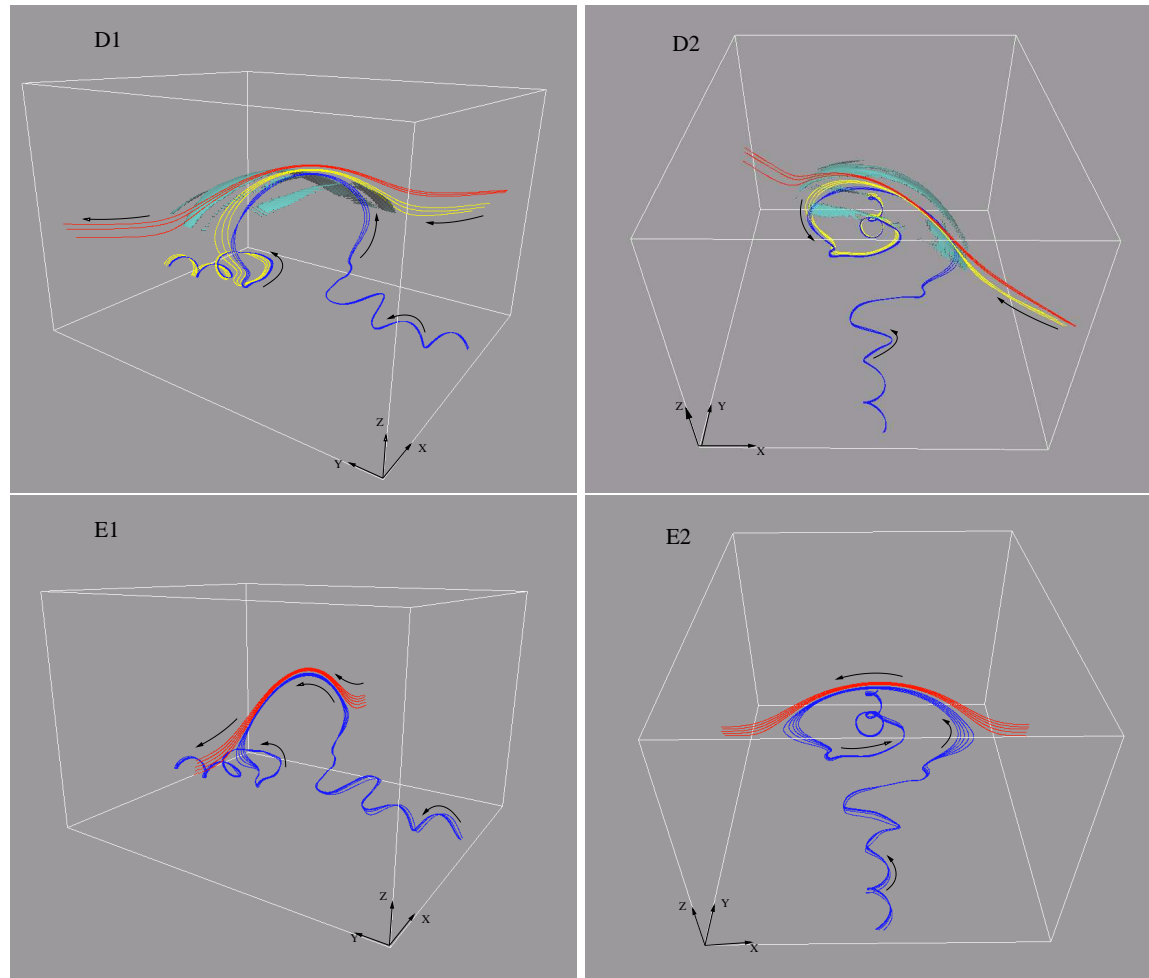


Fig. 16.— Same as in Fig.15 but for the experiments D and E.